Pyrene-Fused Hexaarylbenzene Luminogens: Synthesis, Characterization, and Aggregation-Induced Emission Enhancement

Chuan-Zeng Wang [a, b, *], Ze-Dong Yu [a], Wen-Xuan Zhao [a], Yuki Noda [b], Yi Zhao [a], Xing Feng[c,*], Mark R.J. Elsegood [d], Simon J. Teat [e], Carl Redshaw [f], Takehiko Yamato [b,*]

a. School of Chemical Engineering, Shandong University of Technology, Zibo 255049, P. R. China

b. Department of Applied Chemistry, Faculty of Science and Engineering, Saga University Honjo-machi 1, Saga 840-8502 Japan

c. Guangdong Provincial Key Laboratory of Functional Soft Condensed Matter, School of Material and Energy, Guangdong University of Technology, Guangzhou 510006, P. R. China.

d. Chemistry Department, Loughborough University, Loughborough, LE11 3TU, UK

e. Advanced Light Source, Lawrence Berkeley National Lab, 1 cyclotron Rd, Berkeley, CA 94720, USA

f. Department of Chemistry, The University of Hull, Cottingham Road, Hull, Yorkshire HU6 7RX, UK

*Corresponding author

E-mail: 13639028944@163.com, yamatot@cc.saga-u.ac.jp, hyxhn@sina.com

ABSTRACT: Six novel pyrene-fused hexaarylbenzene derivatives (**3a-f**) were designed, synthesized, and characterized, which exhibited aggregation-induced emission enhancement (AIEE) in the aggregated state by means of THF/H_2O mixtures. Techniques such as theoretical calculations, single crystal X-ray diffraction, and photophysical measurements in solution and in the solid state were employed to illustrate the tunable, variable, and sensitive AIEE features in this system. Both theoretical and experimental results revealed that the nature of the multiple photoluminescence should be taken into account when elucidating and designing multiple photoluminescence phenomenon and molecules.

Keywords: Hexaarylbenzene; Pyrene chemistry; Synthesis & design; Aggregation-induced emission enhancement; Luminescence

1. Introduction

Aggregation-induced emission luminogens (AIEgens) [1–4] based on prototypical analogues of hexaphenylsilole (HPS) [5,6], tetraphenylethene (TPE) [7–9] or 10,10′,11,11′-tetrahydro-5,5′-bidibenzo[a,d][7]annulenylidene (THBA) [10,11] have been, and continue to be, one of the most fundamental and indispensable elements of material science and also in industrial fields. Their excellent performance in the aggregated state and the cutting-edge innovative applications in field of science such as luminescent sensors,

optical devices, phototherapy, and bioimaging are enabling new research directions in molecular design, applied exploration, and elucidation of mechanisms [12–14]. In this context, numerous AIEgens possessing excellent performance have been designed and prepared, which benefit from the growing understanding of the underlying mechanisms for this type of fluorescent molecule [1,7]. Propeller-type hexaarylbenzene (HAB) derivatives as one of the important construction units has enormously enriched the AIEgens family [15].

Recently, a variety of pyrene-based AIEgens were reviewed by Feng and co-workers systematically [16]. It is well known that pyrene and its derivatives belong to the family of polycyclic aromatic hydrocarbons (PAHs), which possess excellent stability and fluorescence efficiency [17,18]. However, the large π-conjugated structure has limited their applications in organic optoelectronic materials because of the aggregation-induced quenching (ACQ) in concentrated solutions and in films or the solid state [19–21]. Thus, great efforts have been made by researchers to reduce or eliminate the ACQ effect. Generally, minimizing the impact by employing bulky groups has become the main strategy, and this can effectively improve the fluorescence efficiency in the solid state by restricting the formation of excimer or π-π interactions [17,22]. On the other hand, benefiting from the establishment of the AIE concept, and the competitive edge in the field of organic optoelectronic materials, the construction of pyrene-based luminescence materials combined with typical AIEgen units or non-typical AIEgen units, has recently attracted considerable efforts [23–27]. For example, from the synthesis of a tetraphenylethylene (TPE) fused pyrene emitter, Zhao and co-workers for the first time [28], to TPE-like pyrene-based AIEgens [29–31], pyrene fused vinylene-based AIEgens [32,33], pyrene-based chalcone AIEgen [34], and other AIE systems [35–37]. All such pyrene-based AIEgens present potential applications in organic light-emitting diodes (OLEDs), sensors, bioimaging, and beyond [38–41].

In our previous work, two pyrene-fused propeller-shaped HAB derivatives were reported with multiple photoluminescence properties [42], and this provided a novel strategy to construct multi-colour luminogens. Thus, this strategy is expected to be used to synthesize single molecule luminescent materials with white emission compared with other emission mechanisms [43]. Herein, we present a series of new HAB derivatives **3a-f**, in which a pyrene unit and a *para*-substituted phenyl group were employed in a HAB scaffold (Scheme 1). The structure-property relationships of the pyrene-based HAB derivatives were investigated and interpreted, which indicated the potential to achieve multiple emission emitters.

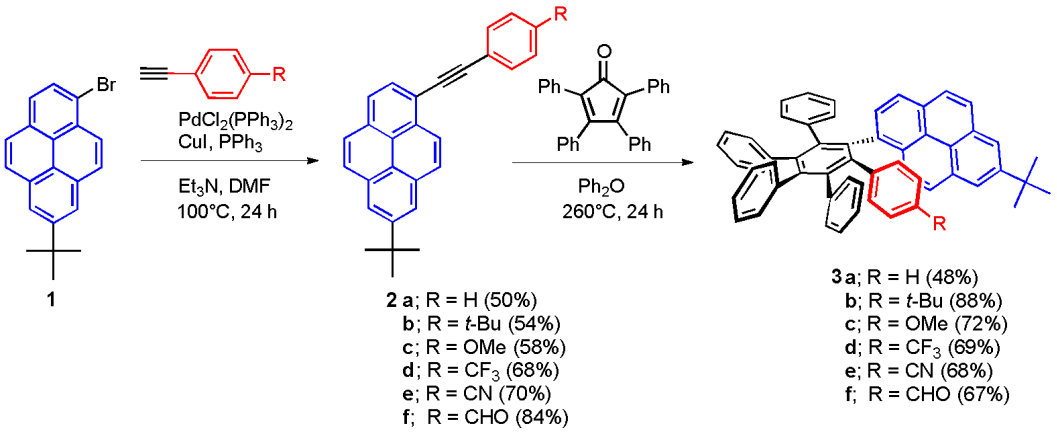

Scheme 1. Synthetic route to compounds **3a-f**.

2. Results and discussion

The pyrene-based HAB derivatives **3a-f** were synthesized in reasonable yield by employing a Sonogashira coupling and Diels-Alder reaction, respectively. The synthetic procedures are provided in the experimental section. All compounds **2a-f** and **3a-f** were characterized by $^{1}H/^{13}C$ NMR spectroscopies, high-resolution mass spectrometry, and X-ray crystallography (see Figs. S1–S24 in the Supporting Information). Meanwhile, all compounds exhibited high thermal stability and excellent solubility.

Single crystals of **3b** and **3c** were prepared from dichloromethane/hexane or chloroform/methanol mixtures, respectively, by slow solvent evaporation, and were analyzed by single crystal X-ray diffraction. Synchrotron radiation was employed for **3b** due to the small crystal size. Detailed information is summarized in Fig. 1, Figs. S25–S26, and Table S1. The twist angles between the central C_6 aromatic core and the attached propeller blades are given below: 70.14(2)° (C1 > C16), 63.08(3)° (C27 > C32), 65.75(3)° (C37 > C42), 59.03(3)° (C43 > C48), 58.64(3)° (C49 > C54), 69.23(3)° (C55 > C60) for **3b**, and 71.38(4)° (C1 > C16), 64.50(4)° (C27 > C32), 64.76(6)° (C34 > C39), 61.63(6)° (C40 > C45), 53.18(5)° (C46 > C51), 64.08(5)° (C52 > C57) for **3c**, respectively. The biggest twist angles in these compounds are more than 70°, which are attributed to the *tert*-butyl substituted pyrene moiety and intermolecular interactions.

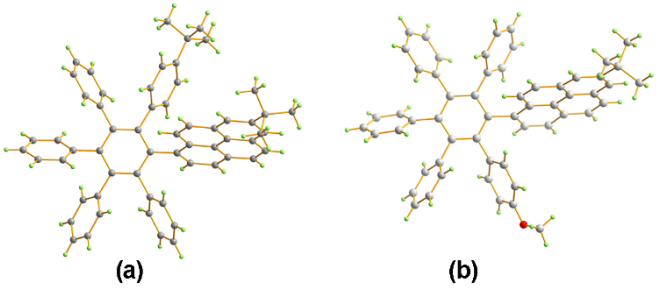

Fig. 1. Crystal structures of **3b** (a) and **3c** (b).

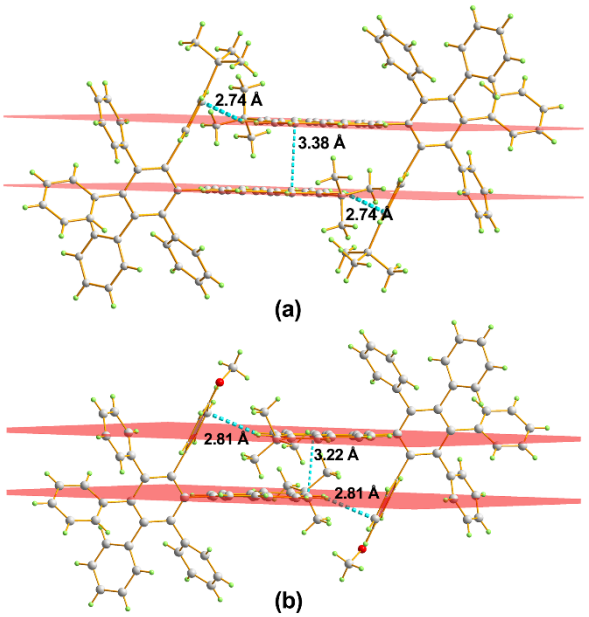

Fig. 2. Packing structures of **3b** (a) and **3c** (b), with principal intermolecular packing interactions.

The detailed intermolecular packing interactions were investigated on the basis of the X-ray crystallography results, and the two compounds present similar spatial arrangements (see Fig. 2). Specifically, for **3b**, the π···π stacking interaction between centro-symmetrically related rings (C1 > C16) have a vertical distance of 3.38 Å. For **3c**, where the OMe group is disordered over two sets of positions on rings either side of the pyrene moiety, we discuss the packing interactions based on the major component, with the OMe group located at C(30) with 58.2(3)% occupancy. The pyrene group exhibited only partial overlap with significant slippage, and the π···π stacking interaction between the edges of pyrene moieties exhibits a shorter vertical distance of 3.22 Å. The π···π stacking interactions play a dominant role in the emission properties. There are also some weak C–H···π interactions in both crystals. In crystal **3b**, the most noteworthy of these being a short contact between the peripheral *tert*-butyl substituted C_6 ring and H(4') at a distance of 2.74 Å. The distance is 2.81 Å between the methoxy substituted C_6 ring and H(16') in crystal **3c**. All of the packing interactions provide significant evidence to interpret the versatile emission behaviour in the

different physical states.

Systematic investigation of the UV-Vis absorption and emission properties was performed in different solvents and in the solid state at room temperature, and the key spectroscopic parameters are depicted in Table 1. As shown in Fig. 3, the six compounds exhibited similar absorption properties, including two sets of distinct, wide shoulder absorption bands at around 273–285 nm, and 334–352 nm. The high-energy shoulder absorption band was centered at around 273–285 nm, with gradually increasing molar absorption coefficients from **3a** to **3f**, which originate from the functionalized pyrene unit. The other low-energy shoulder absorption bands at around 334–352 nm are ascribed to the intramolecular charge-transfer (ICT) between the HAB scaffold and the pyrene moiety. In contrast, a large influence of the substituents at the *para*-position of the substituted C_6 ring to the short-wavelength absorption band (from 36113 $cm^{-1}M^{-1}$ for **3a** to 57981 $cm^{-1}M^{-1}$ for **3f**) was observed. On the other hand, a small influence of the molar absorption coefficients was observed at the long-wavelength absorption band, which indicates that limited intramolecular electronic communication between the pyrene moiety and the HAB scaffold was observed in this system.

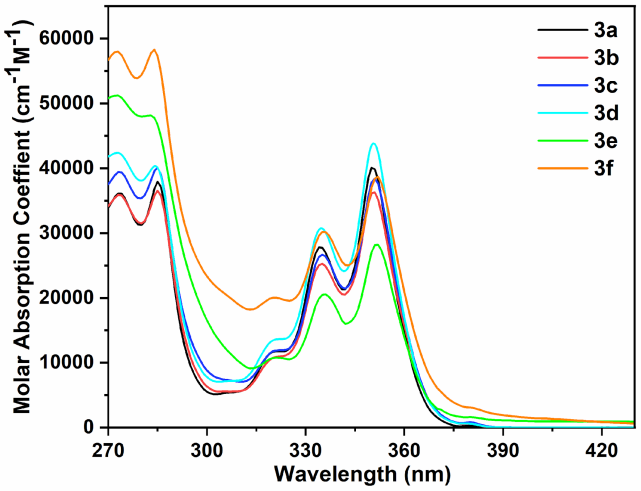

Fig. 3. UV-Vis absorption spectra in DCM solution of compounds **3a**–**f**.

Table 1 The photophysical properties of compounds **3a**–**f**.

R	λ_{abs} (nm) sol[a] [ε (mM^{-1} cm^{-1})]	λ_{em} (nm) Sol[a]/solid[b]	HOMO (eV)[c]	LUMO (eV)[c]	E_g (eV)[c]	HOMO (eV)[d]	LUMO (eV)[e]	E_g (eV)[f]	Φ_{FL}(%) Sol[a]/solid[b]
3a	285 (37.9), 350 (40.1)	395/420	–5.11	–1.39	3.72	–5.49	–2.38	3.11	13/43
3b	285 (36.5), 351 (36.3)	394/424	–5.09	–1.39	3.70	–5.58	–2.52	3.06	18/30
3c	285 (40.1), 351 (38.4)	394/426&437	–5.06	–1.36	3.70	–5.36	–2.35	3.03	12/9

3d	285 (40.3), 351 (43.8)	394/419	–5.20	–1.50	3.70	–5.89	–2.81	3.08	12/26
3e	283 (48.1) 352 (28.2)	386&403/403	–5.28	–1.60	3.68	–5.95	–2.97	2.98	9/10
3f	284 (58.3), 352 (38.7)	394&499/--	–5.20	–1.63	3.57	–5.73	–2.85	2.88	1/3

[a] Measured in dichloromethane at room temperature. [b] Measured as a solid. [c] DFT/B3LYP/6-31G* using Gaussian. [d] Measured from the oxidation potential in CH_2Cl_2 solution by cyclic voltammetry. [e] Calculated from HOMO + E_g. [f] Estimated from the absorption edge of UV-Vis spectra.

The photoluminescence (PL) spectra of **3a**–**f** were recorded in different dilute organic solutions, THF/H_2O mixtures and in the solid state. As shown in Fig. 4, compared with the similar absorption spectra of the six compounds, the emission spectra present distinct differences in solution, especially that for compound **3f**. Specifically, with the change of substituent at the *para*-position of C_6 ring, there is no obvious shift around the blue emission region, but an obvious shoulder emission peak is observed from **3d** to **3f**. Meanwhile, a new bathochromic-shift emission is visible, centered at 499 nm for **3f**, which can be attributed to the excimer emission, and the more distinct electronic interaction of the HAB scaffold with the electron withdrawing –CHO group and pyrene core [44]. In order to evaluate the effect of the substituents at the *para*-position of the C_6 ring, different solvents with various polarities were employed to investigate the emission properties of **3e** and **3f** (see Fig. S27 in the Supporting Information). The emission spectra of **3e** present a slight solvent dependence, which indicates that a weak intramolecular charge-transfer phenomenon or sensitivity could exist. In sharp contrast, **3f** exhibited marked differences in the emission spectra, with the emission band at 499 nm being dramatically enhanced from cyclohexane to DMF solution, which can be attributed to the strong electron-withdrawing ability of the –CHO group and the increase of the intermolecular π···π and C-H···O interactions [45], which also results in a distinct weakening of the monomer emission at 394 nm on increasing the solvent polarity [46]. The fluorescence quantum yields (Φ_F) were recorded in dilute solution, and all compounds exhibit low Φ_F values, indicating that the non-radiative decay plays a dominant role due to the free intramolecular rotations of the peripheral phenyls [1]. Notably, **3f** displayed the lowest fluorescence quantum yield, and this may result from through-space charge transfer (TSCT) [47] and the formation of π-π interactions between the neighboring pyrene moieties.

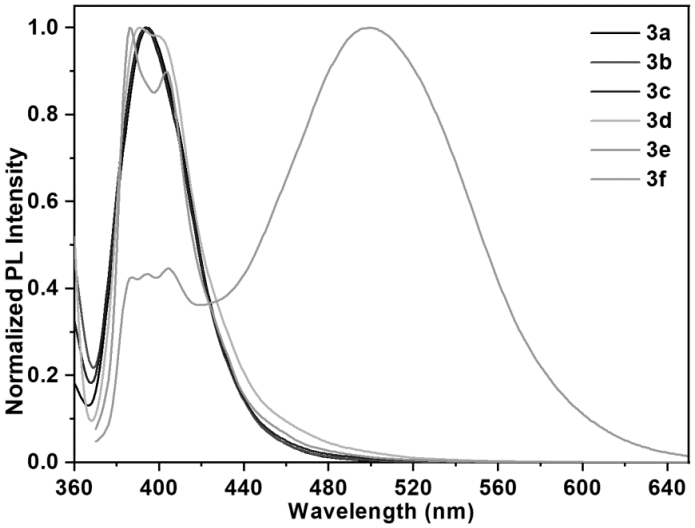

Fig. 4. Fluorescence spectra in DCM solution of compounds **3a-f**.

These pyrene-fused HAB derivatives were further investigated in THF/H_2O mixtures at 50 μM. Comparing with the traditional pyrene-based ACQ luminogens in the aggregated state, these compounds exhibit an obvious aggregation-induced emission enhancement (AIEE) property at different water fractions (f_w). As shown in Fig. 5 and Figs. S28–31, the six compounds present similar emission behaviour with about a 3-fold enhancement in the aggregated state over the pure THF solutions. Taking **3a** and **3f** as representative examples, the PL intensity in the blue region with a wide shoulder peak is enhanced on gradual addition of the water fraction to 60%, which indicates extensive intermolecular C−H···π interactions restrict the rotational motions of the peripheral phenyl rings and the formation of aggregations. The enhancement was interrupted on further increase of the f_w beyond 60%. For compound **3a** (as shown in Figs. 5a, 5b), the type of emission curve remained unaltered when the f_w was beyond 70%. In the case of an overall decrease, the peak on the left of the shoulder weakened gradually and the other peak increased relatively, with a gradual bathochromic-shift in water-dominated solvents (70% < f_w < 99%), which may be ascribed to the change of interaction types in different aggregation forms [48–50]. On the other hand, the fluorescence intensities of **3f** in THF/H_2O mixtures exhibited a distinct difference when compared with **3a**–**e**. The short-wavelength emission band at around 394 nm presents a similar trend to **3a**–**e**, while complex changes were observed at the long-wavelength emission band, with the fluorescence intensity enhanced over the pure THF solution to f_w = 10%, and the emission band gradually became weak in the range of 10%–70%. On further increasing the f_w, a new round of enhancement and weakening was observed again from 70%–80% and 80%–99%, respectively. This may be ascribed to the different molecular aggregates forming

in the presence of different f_w [51]. As mentioned above, the packing forms of **3b** and **3c** in the aggregated state supported the proposed mechanism, with obvious C−H···π and π···π stacking interactions between the two phenyl groups and two pyrenyl groups being observed in the crystalline state. More variable intra/intermolecular interactions may affect the non-radiative relaxation process.

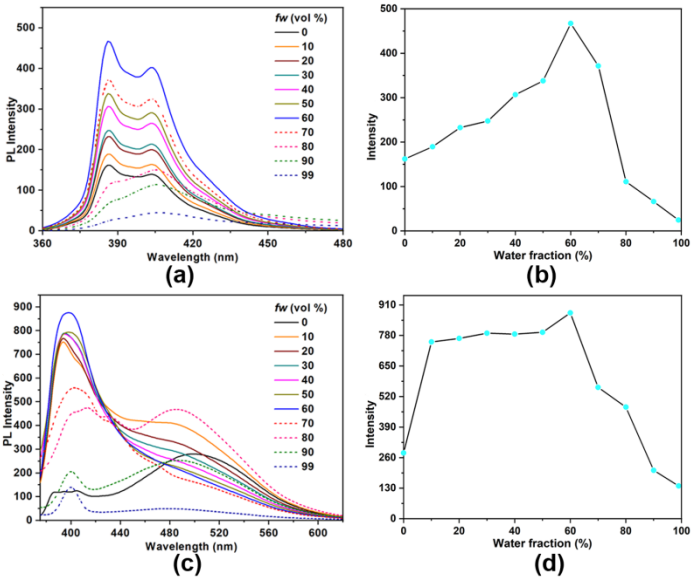

Fig. 5. (a), (c) PL spectra of **3a** and **3f** in THF/water mixtures with different water fractions (fw), respectively. (b), (d) Plot of PL intensity at different fractions (0–99 vol%) for **3a** and **3f**.

As shown in Fig. 6, more enhanced emissions were present in the amorphous state rather than in the pure organic solutions. Almost all of the compounds, except **3c**, exhibited high quantum yields in the solid state, with all the emission bands centered at 403–437 nm. The results demonstrated that monomeric emission plays a dominant role [52], indicating that C−H···π interactions rather than π···π interactions are formed in this system.

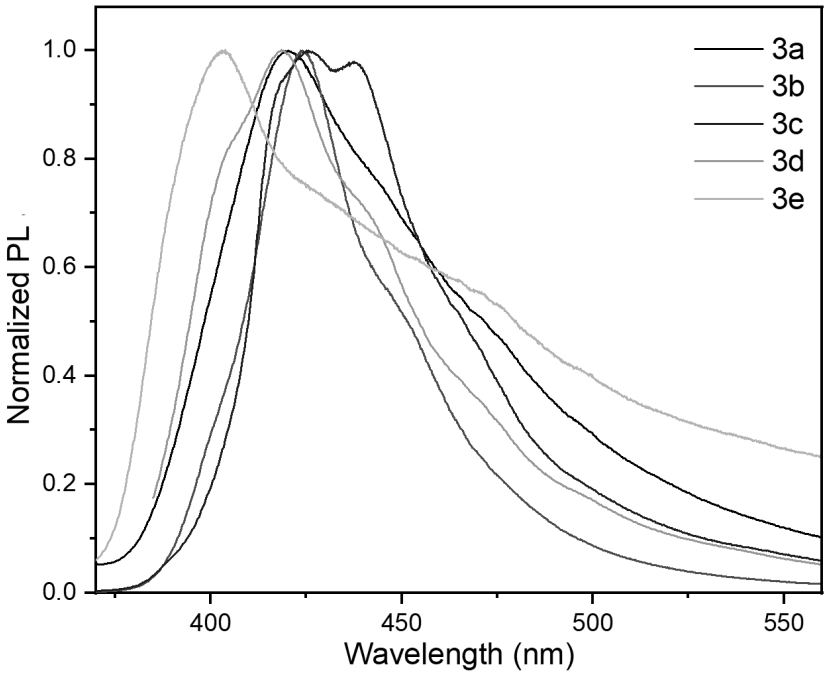

Fig. 6. PL spectra of compounds **3a-e** in the solid state.

DFT calculations (B3LYP/6-31G*) were carried out to evaluate the electron delocalization in compounds **3a-f**. As shown in Fig. 7, HOMOs of TSCT in the HAB scaffolds are mainly localized on the pyrenyl donors, while LUMOs are distributed on pyrenyl and strong electron-withdrawing groups, which is mainly reflected in the latter two compounds. Owing to the discrepant HOMO and LUMO distributions of **3e** and **3f**, a gradually reducing band gap energy (E_g) is gradually observed from **3a** to **3f**. Subsequently, cyclic voltammetry (CV) were carried out to elucidate the electronic states. As shown in Fig. S32, the six compounds present irreversible redox processes with obvious positive potentials. Further estimation of the frontier orbital analysis using experimental results indicated that the trend of DFT calculation results are in good agreement with the estimated values from UV spectra and oxidation potential. The results of these calculations are also consistent with the emission properties described above, so this work demonstrated a viable strategy that can be employed for the rationally design of novel luminogens with multicolour emission and even white-light emission properties [53].

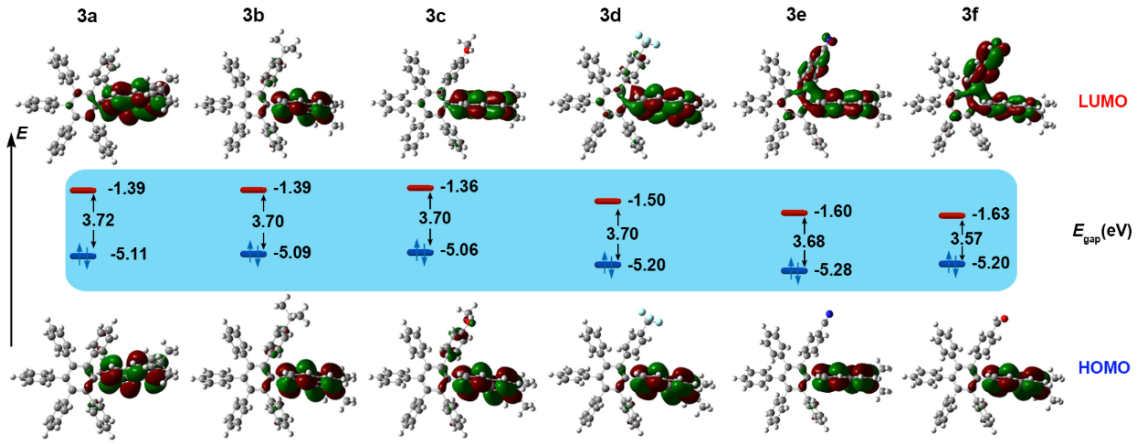

Fig. 7. Frontier-molecular-orbital distributions and energy levels diagram of **3a-f** by DFT calculations.

3. Experimental section

3.1. General procedures

The synthetic route to the compounds **3a-f** is shown in Scheme 1. All reactions were carried out under a dry argon atmosphere. Solvents were Guaranteed reagent (GR) grade for cyclohexane, 1,4-dioxane, tetrahydrofuran (THF), dichloromethane (CH_2Cl_2), and dimethylformamide (DMF), and stored over molecular sieves. Other reagents were obtained commercially and were used without further purification. Reactions were monitored using thin layer chromatography (TLC). Commercial TLC plates (Merck Co.) were developed and the spots were identified under UV light at 254 and 365 nm. Column chromatography was performed on silica gel 60 (0.063-0.200 mm). All synthesized compounds were characterized using ^{1}H-NMR, ^{13}C-NMR spectroscopy, and HRMS (FAB) mass analysis and target compounds were characterized by X-ray crystallography. UV/vis spectra were recorded with a UV/vis/NIR spectrometer in various organic solvents. Fluorescence spectroscopic studies were performed in various organic solvents in a semimicro fluorescence cell (Hellma®, 104F-QS, 10 × 4 mm, 1400 μL) with a Varian Cary Eclipse spectrophotometer. Fluorescence quantum yields were measured using absolute methods. The ground-state geometries were optimized using density functional theory (DFT) with the B3LYP hybrid functional at the basis set level of 6-31G(d,p). All the calculations were carried out in the gas phase using the Gaussian 09 program.

3.2. Experimental details

3.2.1. Synthesis of compounds **2a–f**

The series of compounds **2a**–**f** was synthesized from 7-*tert*-butyl-1-bromopyrene **1** [54] with the corresponding aryl alkyne by a Sonogashira coupling reaction.

7-*tert*-Butyl-1-(4-methoxyphenylethynyl)pyrene (2c). To a stirred solution of 7-*tert*-butyl-1-bromopyrene **1** (300 mg, 0.890 mmol), Et_3N (10 mL) and DMF (10 mL), was added 4-methoxyphenyl acetylene (235 mg, 1.78 mmol) and PPh_3 (37.0 mg, 0.142 mmol), and the mixture was stirred at room temperature under argon. $PdCl_2(PPh_3)_2$ (46.0 mg, 0.062 mmol), and CuI (19 mg, 0.098 mmol) were then added, and the mixture was heated to 100 °C with stirring for 24 h. After it was cooled, the mixture was diluted into CH_2Cl_2 (50 mL) and washed successively with saturated aqueous $NH_4Cl{\cdot}H_2O$ and brine. The organic extracts were dried with $MgSO_4$ and evaporated. The residue was purified by column chromatography eluting with (CH_2Cl_2/hexane, 1:1) to give **2c** as a light yellow solid. Recrystallization from hexane gave 7-*tert*-butyl-1-(4-methoxyphenylethynyl)pyrene **2c** (200 mg, 58 %) as a colourless solid. M.p. 159–160°C; ^{1}H NMR (400 MHz, $CDCl_3$): δ_H = 1.50 (s, 9H, *t*Bu), 3.88 (s, 3H, OMe), 6.97 (d, *J* = 8.8 Hz, 2H, Ar-*H*), 7.67 (d, *J* = 9.0 Hz, 2H, Ar-*H*), 8.01–8.11 (m, 3H, pyrene-*H*), 8.16 (dd, *J* = 9.3, 3.1 Hz, 2H, pyrene-*H*), 8.24 (d, *J* = 6.0 Hz, 2H, pyrene-*H*), 8.63 ppm (d, 1H, *J* = 9.2 Hz, pyrene-*H*); ^{13}C NMR (100 MHz, $CDCl_3$): δ_C = 31.9, 35.3, 55.4, 87.5, 95.0, 114.1, 115.7, 118.0, 122.6, 122.8, 124.3, 124.4, 125.5, 127.1, 128.2, 128.4, 129.1, 130.8, 131.0, 131.1, 131.6, 133.2, 149.4, 159.7 ppm; FAB-MS: m/z calcd for $C_{29}H_{24}O$ 388.18 [M^+]; found 388.24 [M^+]; Found: C, 89.88; H, 6.39%; molecular formula $C_{28}H_{22}$ requires C, 89.66; H, 6.23%.

A similar procedure using phenylacetylene, 4-*tert*-butylphenylacetylene, 4-(trifluoromethyl)phenylacetylene, 4-cyanophenyacetylene, and 4-ethynylbenzaldehyde was followed for the synthesis of **2a**–**f**.

7-*tert*-Butyl-1-phenylethynylpyrene (2a) was obtained as a colourless solid (recrystallized from hexane, 159 mg, 50%). M.p. 171–173°C; ^{1}H NMR (400 MHz, $CDCl_3$): δ_H = 1.59 (s, 9H, *t*Bu), 7.39–7.46 (m, 3H, Ar-*H*), 7.73 (d, *J* = 7.9 Hz, 2H, Ar-*H*), 8.01–8.11 (m, 3H, pyrene-*H*), 8.16 (s, 1H, pyrene-*H*), 8.18 (s, 1H, pyrene-*H*), 8.25 (d, *J* = 6.4 Hz, 2H, pyrene-*H*), 8.64 ppm (d, *J* = 8.9 Hz, 1H, pyrene-*H*); ^{13}C NMR (100 MHz, $CDCl_3$): δ_C = 31.9, 35.3, 88.8, 94.9, 117.5, 122.6, 122.9, 122.9, 123.6, 124.3, 124.4, 125.4, 127.1, 128.4, 128.5, 128.5, 129.3, 130.9, 131.1, 131.7, 131.7, 149.4 ppm; FAB-MS: *m/z* calcd for $C_{28}H_{22}$ 358.17 [M^+]. found 358.24 [M^+]; Found: C, 93.60; H, 6.34%; molecular formula $C_{28}H_{22}$ requires C, 93.81; H, 6.19%.

7-*tert*-Butyl-1-(4-*tert*-butylphenylethynyl)pyrene (2b) was obtained as a pale-green solid (recrystallized from EtOAc/MeOH; 2:8, 201 mg, 54%). M.p. 154–155°C; ^{1}H NMR (400 MHz, $CDCl_3$): δ_H = 1.37 (s, 9H, *t*Bu), 1.59 (s, 9H, *t*Bu), 7.45 (d, *J* = 8.4 Hz, 2H, Ar-*H*), 7.66 (d, *J* = 8.4 Hz, 2H, Ar-*H*), 8.01 (d, *J* = 9.0 Hz, 1H, pyrene-*H*), 8.07 (d, *J* = 8.9 Hz, 1H, pyrene-*H*), 8.09 (d, *J* = 8.0 Hz, 1H, pyrene-*H*), 8.15 (s, 1H, pyrene-*H*), 8.17 (s, 1H, pyrene-*H*), 8.24 (dd, *J* = 7.9, 1.7 Hz, 2H, pyrene-*H*), 8.63 ppm (d, *J* = 9.0 Hz, 1H, pyrene-*H*); ^{13}C NMR (100 MHz, $CDCl_3$): δ_C = 31.2, 31.9, 34.9, 35.3, 88.1, 95.1, 117.8, 120.6, 122.6, 122.8, 124.3, 124.4, 125.5, 127.1, 128.2, 128.4, 129.2, 131.0, 131.1, 131.4, 131.7, 149.4, 151.7 ppm; FAB-MS: *m/z* calcd for $C_{32}H_{30}$ 414.23 [M^+]; found 414.36 [M^+]; Found: C, 92.99; H, 7.57%; molecular formula $C_{32}H_{30}$ requires C, 92.71; H, 7.29%.

7-*tert*-Butyl-1-(4-trifluoromethylphenylethynyl)pyrene (2d) was obtained as light green needles (recrystallized from hexane, 257 mg, 68%). M.p. 205–206°C; ^{1}H NMR (400 MHz, $CDCl_3$): δ_H = 1.60 (s, 9H, *t*Bu), 7.68 (d, *J* = 8.0 Hz, 2H, Ar-*H*), 7.82 (d, *J* = 8.0 Hz, 2H, Ar-*H*), 8.03 (d, *J* = 9.0 Hz, 1H, pyrene-*H*), 8.10 (d, *J* = 9.2 Hz, 1H, pyrene-*H*), 8.11 (d, *J* = 8.0 Hz, 1H, pyrene-*H*), 8.16–8.20 (m, 2H, pyrene-*H*), 8.27 (dd, *J* = 7.5, 1.7 Hz, 2H, pyrene-*H*), 8.60 ppm (d, *J* = 9.2 Hz, 1H, pyrene-*H*); ^{13}C NMR (100 MHz, $CDCl_3$): δ_C = 31.9, 35.3, 91.2, 93.4, 116.6, 122.5, 123.1, 124.4, 125.1, 125.4, 127.1, 127.4, 128.7, 128.8, 129.4, 129.8, 130.9, 131.1, 131.5, 131.9, 131.9, 149.6 ppm; FAB-MS: *m/z* calcd for $C_{29}H_{21}F_3$ 426.16 [M^+]; found 426.27 [M^+]; Found: C, 81.94; H, 5.12%; molecular formula $C_{29}H_{21}F_3$ requires C, 81.67; H, 4.96%.

7-*tert*-Butyl-1-(4-cyanophenylethynyl)pyrene (2e) was obtained as a white solid (recrystallized from hexane, 120 mg, 70%). M.p. 211–212°C; ^{1}H NMR (400 MHz, $CDCl_3$): δ_H = 1.60 (s, 9H, *t*Bu), 7.70 (d, *J* = 8.0 Hz, 2H, Ar-*H*), 7.78 (d, *J* = 8.5 Hz, 2H, Ar-*H*), 8.04 (d, *J* = 8.9 Hz, 1H, pyrene-*H*), 8.12 (d, *J* = 8.4 Hz, 2H, pyrene-*H*), 8.15–8.22 (m, 2H, pyrene-*H*), 8.28 (d, *J* = 9.2 Hz, 2H, pyrene-*H*), 8.57 ppm (d, *J* = 9.1 Hz, 1H, pyrene-*H*); ^{13}C NMR (100 MHz, $CDCl_3$): δ_C = 31.9, 35.3, 93.2, 93.3, 111.3, 116.2, 118.6, 122.4, 123.2, 123.3, 124.3, 124.4, 125.0, 127.0, 128.4, 128.9, 128.9, 129.5, 130.8, 131.0, 131.7, 132.0, 132.0, 132.0, 132.1, 149.6 ppm; FAB-MS: *m/z* calcd for $C_{29}H_{21}N$ 383.1674 [M^+]; found 383.1676 [M^+].

7-*tert*-Butyl-1-(4-formylphenylethynyl)pyrene (2f) was obtained as a yellow solid (recrystallized from hexane, 124 mg, 84%). M.p.167–168°C; ^{1}H NMR (400 MHz, $CDCl_3$): δ_H = 1.60 (s, 9H, *t*Bu), 7.86 (d, *J* = 5.0 Hz, 2H, Ar-*H*), 7.933 (d, *J* = 4.8 Hz, 2H, Ar-*H*), 8.05 (s, 1H, pyrene-*H*), 8.08–8.13 (m, 2H, pyrene-*H*), 8.16–8.22 (m, 2H, pyrene-*H*), 8.28 (d, *J* = 10.4 Hz, 2H, pyrene-*H*), 8.61 ppm (d, *J* = 9.1 Hz, 1H, pyrene-*H*), 10.06 ppm (s, *J* = 2.5 Hz, 1H,

CHO); ^{13}C NMR (100 MHz, $CDCl_3$): δ_C = 31.9, 35.3, 76.7, 77.0, 77.3, 93.1, 94.1, 116.5, 122.5, 123.2, 124.4, 125.1, 127.1, 128.8, 129.6, 130.9, 131.1, 131.6, 132.1, 135.4, 149.6, 191.4 ppm; FAB-MS: *m/z* calcd for $C_{29}H_{22}O$ 386.1671 [M^+]; found 386.1716 [M^+].

3.2.2. Synthesis of compounds **3a–f**

The series of compounds **3a–f** was synthesized from 2,3,4,5-tetraphenylcyclopenta-2,4-dienone with the corresponding 1-arylethynyl-7-*tert*-butylpyrenes (**2a–f**) by a Diels−Alder reaction.

1-(7-*tert*-Butyl-pyren-1-yl)-2,3,4,5,6-(pentaphenyl)benzene (3a). Compound **2a** (100 mg, 0.279 mmol) and 2,3,4,5-tetraphenylcyclopenta-2,4-dienone (161 mg, 0.419 mmol) were dissolved in Ph_2O (1.0 mL) under inert-gas atmosphere. The mixture was refluxed for 24 h, and then the solvent was removed *in vacuo*. The residue was purified by column chromatography on silica gel (CH_2Cl_2/ hexane 4:6) as eluent to give a colourless solid. Recrystallization from CH_2Cl_2/ hexane (1:9, v/v) gave 1-(7-*tert*-butyl-pyren-1-yl)-2,3,4,5,6-(pentaphenyl)benzene **3a** (95.7 mg, 48%) as a colourless solid. M.p. 318–320°C; ^{1}H NMR (400 MHz, $CDCl_3$): δ_H = 1.55 (s, 9H, *t*Bu), 6.38 (t, *J* = 7.5 Hz, 2H, Ph-*H*), 6.48 (t, *J* = 7.4 Hz, 2H, Ph-*H*), 6.63 (t, *J* = 7.4 Hz, 2H, Ph-*H*), 6.70 (d, *J* = 7.5 Hz, 2H, Ph-*H*), 6.83–6.98 (m, 17H, Ph-*H*), 7.64 (d, *J* = 7.9 Hz, 1H, pyrene-*H*), 7.73 (d, *J* = 7.9 Hz, 1H, pyrene-*H*), 7.79 (d, *J* = 9.0 Hz, 1H, pyrene-*H*), 7.86 (d, *J* = 9.0 Hz, 1H, pyrene-*H*), 7.91 (d, *J* = 9.3 Hz, 1H, pyrene-*H*), 8.06 (d, *J* = 9.2 Hz, 1H, pyrene-*H*), 8.10 (s, 1H, pyrene-*H*), 8.11 ppm (s, 1H, pyrene-*H*); ^{13}C NMR (100 MHz, $CDCl_3$): δ_C = 31.9, 35.1, 121.74 121.9, 122.8, 123.2, 123.9, 125.1, 125.2, 125.2, 126.0, 126.4, 126.5, 126.6, 126.6, 127.4, 129.3, 129.4, 129.5, 130.3, 130.7, 130.9, 131.0, 131.5, 131.5, 131.6, 136.3, 138.8, 140.3, 140.4, 140.6, 140.7, 141.5, 148.6 ppm; FAB-MS: *m/z* calcd for $C_{56}H_{42}$ 714.3287 [M^+]; found 714.3266 [M^+].

A similar procedure using compounds **2b–f** was followed for the synthesis of **3b–f**.

1-(7-*tert*-Butyl-pyren-1-yl)-2-(4-*tert*-butylphenyl)-3,4,5,6-(tetraphenyl)benzene (3b) was obtained as a colourless solid (recrystallized from CH_2Cl_2/ hexane (1:9, v/v)), (yield, 88%). M.p. 327–329°C; ^{1}H NMR (400 MHz, $CDCl_3$): δ_H = 1.55 (s, 9H, *t*Bu), 6.40 (t, *J* = 7.5 Hz, 2H, Ph-*H*), 6.48 (t, *J* = 7.4 Hz, 2H, Ph-*H*), 6.59 (t, *J* = 7.4 Hz, 2H, Ph-*H*), 6.72 (d, *J* = 7.5 Hz, 2H, Ph-*H*), 6.85–6.93 (m, 16H, Ph-*H*), 7.62 (d, *J* = 7.9 Hz, 1H, pyrene-*H*), 7.72 (d, *J* = 7.9 Hz, 1H, pyrene-*H*), 7.81 (d, *J* = 9.0 Hz, 1H, pyrene-*H*), 7.85 (d, *J* = 9.0 Hz, 1H, pyrene-*H*), 7.91 (d, *J* = 9.3 Hz, 1H, pyrene-*H*), 8.05 (d, *J* = 9.2 Hz, 1H, pyrene-*H*), 8.08 (s, 1H, pyrene-*H*), 8.10 ppm (s, 1H, pyrene-*H*); ^{13}C NMR (100 MHz, $CDCl_3$): δ_C = 33.8, 35.1,

121.6, 121.7, 122.8, 123.2, 124.0, 125.0, 125.1, 125.1, 125.2, 126.0, 126.3, 126.4, 126.5, 126.6, 126.7, 127.3, 129.3, 129.3, 129.6, 130.0, 130.5, 130.7, 130.9, 131.5, 131.6, 136.5, 137.1, 138.9, 140.2, 140.3, 140.5, 140.6, 140.7, 140.8, 141.4, 141.7, 147.6, 148.5 ppm; FAB-MS: *m/z* calcd for $C_{60}H_{50}$ 770.3913 [M^+]; found 770.3946 [M^+].

1-(7-*tert*-Butyl-pyren-1-yl)-2-(4-methoxyphenyl)-3,4,5,6-(tetraphenyl)benzene (3c) was obtained as a colourless solid (recrystallized from CH_2Cl_2/ hexane (2:8, v/v)), (yield, 72%). M.p. 281–283°C; ^{1}H NMR (400 MHz, $CDCl_3$): δ_H = 1.55 (s, 9H, *t*Bu), 3.34 (s, 3H, OMe), 5.93 (dd, *J* = 8.4 Hz, 2H, Ph-*H*), 6.18 (dd, *J* = 8.5 Hz, 2H, Ph-*H*), 6.37 (t, 2H, Ph-*H*), 6.48 (t, 2H, Ph-*H*), 6.66 (t, *J* = 7.4 Hz, 2H, Ph-*H*), 6.75 (d, *J* = 7.5 Hz, 2H, Ph-*H*), 6.84–6.89 (m, 16H, Ph-*H*), 7.65 (d, *J* = 7.9 Hz, 1H, pyrene-*H*), 7.74 (d, *J* = 7.9 Hz, 1H, pyrene-*H*), 7.83 (d, *J* = 9.0 Hz, 1H, pyrene-*H*), 7.89 (d, *J* = 9.0 Hz, 1H, pyrene-*H*), 7.92 (d, *J* = 9.3 Hz, 1H, pyrene-*H*), 8.05 (d, *J* = 9.2 Hz, 1H, pyrene-*H*), 8.12 ppm (s, 2H, pyrene-*H*); ^{13}C NMR (100 MHz, $CDCl_3$): δ_C =31.9, 35.1, 54.5, 111.7, 121.7, 121.8, 122.8, 123.3, 124.0, 125.1, 125.1, 125.2, 126.0, 126.3, 126.5, 126.6, 127.4, 129.2, 129.3, 129.5, 130.3, 130.7, 130.9, 131.0, 131.4, 131.4, 131.5, 131.9, 132.7, 136.5, 139.0, 140.2, 140.3, 140.6, 140.8, 141.1, 141.5, 148.5, 156.7 ppm; FAB-MS: *m/z* calcd for $C_{57}H_{44}O$ 744.3392 [M^+]; found 744.3386 [M^+].

1-(7-*tert*-Butyl-pyren-1-yl)-2-(4-trifluoromethylphenyl)-3,4,5,6-(tetraphenyl)benzene (3d) was obtained as a colourless solid (recrystallized from CH_2Cl_2/ hexane (2:8, v/v)), (yield, 69%). M.p. 348–349°C; ^{1}H NMR (400 MHz, $CDCl_3$): δ_H = 1.55 (s, 9H, *t*Bu), 6.39 (t, *J* = 7.3 Hz, 2H, Ph-*H*), 6.49 (t, *J* = 7.3 Hz, 2H, Ph-*H*), 6.63 (t, *J* = 7.6 Hz, 2H, Ph-*H*), 6.70 (d, *J* = 7.5 Hz, 2H, Ph-*H*), 6.78–6.93 (m, 16H, Ph-*H*), 7.62 (d, *J* = 7.7 Hz, 1H, pyrene-*H*), 7.74 (d, *J* = 7.6 Hz, 1H, pyrene-*H*), 7.81 (d, *J* = 8.7 Hz, 1H, pyrene-*H*), 7.91 (dd, *J* = 16.5 Hz, 2H, pyrene-*H*), 8.04 (d, *J* = 9.2 Hz, 1H, pyrene-*H*), 8.13 ppm (s, 2H, pyrene-*H*); ^{13}C NMR (100 MHz, $CDCl_3$): δ_C = 31.9, 35.2, 110.0, 121.9, 122.2, 122.8, 123.1, 123.4, 124.0, 125.3, 126.4, 126.6, 126.7, 126.8, 126.9, 127.3, 129.3, 129.6, 130.3, 130.4, 130.6, 130.8, 131.0, 131.1, 131.3, 131.3, 131.4, 135.5, 138.6, 139.9, 140.0, 140.1, 140.3, 140.4, 140.9, 141.0, 141.8, 144.3 ppm; FAB-MS: *m/z* calcd for $C_{57}H_{41}F_3$ 782.3160 [M^+]; found 782.3147 [M^+].

1-(7-*tert*-Butyl-pyren-1-yl)-2-(4-cyanophenyl)-3,4,5,6-(tetraphenyl)benzene (3e) was obtained as a colourless solid (recrystallized from CH_2Cl_2/ hexane (2:3, v/v)), (yield, 68%). M.p. 186–187°C; ^{1}H NMR (400 MHz, $CDCl_3$): δ_H = 1.59 (s, 9H, *t*Bu), 6.44 (t, *J* = 7.4 Hz, 1H, Ph-*H*), 6.55 (t, *J* = 7.4 Hz, 1H, Ph-*H*), 6.68–6.77 (m, 3H, Ph-*H*), 6.82–7.04 (m, 19H, Ph-*H*), 7.64 (d, *J* = 7.8 Hz, 1H, pyrene-*H*), 7.78 (d, *J* = 7.9 Hz, 1H, pyrene-*H*), 7.84 (d, *J* =

8.9 Hz, 1H, pyrene-*H*), 7.91–7.99 (m, 2H, pyrene-*H*), 8.04 (d, *J* = 9.1 Hz, 1H, pyrene-*H*), 8.18 ppm (d, *J* = 2.7 Hz, 2H, pyrene-*H*); ^{13}C NMR (100 MHz, $CDCl_3$): δ_C = 30.9, 34.1, 107.8, 117.8, 121.0, 121.3, 121.6, 122.3, 122.9, 124.4, 124.5, 124.7, 124.7, 125.2, 125.5, 125.6, 125.7, 125.9, 126.0, 126.1, 126.2, 128.1, 128.6, 128.9, 129.1, 129.2, 129.5, 129.7, 129.9, 130.2, 130.3, 130.4, 134.1, 137.4, 138.7, 139.0, 139.1, 140.0, 140.4, 140.8, 144.6, 147.8 ppm; FAB-MS: *m/z* calcd for $C_{57}H_{41}O$ 739.3239 [M^+]; found 739.3235 [M^+].

1-(7-*tert*-Butyl-pyren-1-yl)-2-(4-formylphenyl)-3,4,5,6-(tetraphenyl)benzene (3f) was obtained as a light yellow solid (recrystallized from CH_2Cl_2/ hexane (1:4, v/v)), (yield, 67%). M.p. 170–171°C; ^{1}H NMR (400 MHz, $CDCl_3$): δ_H = 1.55 (s, 9H, *t*Bu), 6.38–6.43 (m, 1H, Ph-*H*), 6.49–6.54 (m, 1H, Ph-*H*), 6.68 (d, *J* = 12.1 Hz, 3H, Ph-*H*), 6.80–6.98 (m, 19H, Ph-*H*), 7.63 (d, *J* = 7.8 Hz, 1H, pyrene-*H*), 7.73 (d, *J* = 7.7 Hz, 1H, pyrene-*H*), 7.79 (d, *J* = 8.9 Hz, 1H, pyrene-*H*), 7.88 (d, *J* = 8.9 Hz, 1H, pyrene-*H*), 7.93 (d, *J* = 9.2 Hz, 1H, pyrene-*H*), 8.04 (d, *J* = 11.2 Hz, 1H, pyrene-*H*), 8.12 (s, 2H, pyrene-*H*), 9.43 ppm (s, 1H, CHO-*H*); ^{13}C NMR (100 MHz, $CDCl_3$): δ_C = 31.9, 35.1, 121.9, 122.2, 122.7, 123.3, 123.9, 125.3, 126.6, 126.7, 126.8, 126.9, 127.3, 128.9, 131.0, 131.2, 131.3, 131.4, 131.4, 133.0, 135.4, 138.4, 139.9, 139.9, 1140.0, 140.2, 140.9, 141.1, 141.7, 147.3, 148.7, 192.0 ppm; FAB-MS: *m/z* calcd for $C_{57}H_{42}O$ 742.3236 [M^+]; found 742.3260 [M^+].

3.3. X-ray Crystallography

Suitable single crystals of **3b** and **3c** were obtained from dichloromethane/hexane or chloroform/methanol solutions, respectively. For **3b**, diffraction data was collected at the ALS, beam line 11.3.1, using silicon 111-monochromated synchrotron radiation (λ = 0.7749 Å). For **3c**, data were collected using a conventional sealed-beam source. Data were corrected for Lorentz and polarisation effects and for absorption from multiple and symmetry equivalent measurements [55]. The structures were solved by a charge flipping algorithm and refined by full-matrix least-squares methods on F^2 [56–58]. For **3c**, the OMe group is disordered over two sets of positions, these are located on two different rings on either side of the pyrene ring. The major component is located at C(30) and is 75.6(4)% occupied. The minor component is located at C(55). The methyl groups on the *t*Bu group at C(17) were modelled as disordered over two sets of positions with major occupancy 74.7(5)%. See Table S1 for crystal data. CCDC-2064691 (**3b**) and CCDC-2064692 (**3c**) contain supplementary crystallographic data for this paper. Copies of the data can be obtained, free of charge, on application to CCDC, 12 Union Road, Cambridge CB2 1EZ, UK [fax: 144-1223-336033 or e-mail: deposit@ccdc.cam.ac.uk].

4. Conclusion

In summary, a series of pyrene-fused hexaarylbenzene luminogens have been designed and characterized. The emission properties of the HAB derivatives **3a-f** were systematically investigated in different states, which indicated that these compounds exhibit both AIEE and ACQ phenomena. The unique photophysical properties of the aggregation-triggered AIEE/ACQ transition with multiple emission bands in a single molecule in THF/H_2O mixtures were interpreted by theoretical and experimental results. More interestingly, all compounds present higher fluorescence quantum yields in the solid state than in the pure organic solution, indicating that the propeller-like molecular configuration can be used to design efficient photoelectric materials with multiple emission properties.

Acknowledgments

This work was performed under the Cooperative Research Program of "Network Joint Research Center for Materials and Devices (Institute for Materials Chemistry and Engineering, Kyushu University)". We would like to thank the Natural Science Foundation of Shandong Province (Grant No. ZR2019BB067) The EPSRC is thanked for an overseas travel grant to C.R. (EP/R023816/1).

References

[1] Mei J, Leung NLC, Kwok RTK, Lam JWY, Tang BZ. Aggregation-induced emission: together we shine, united we soar. Chem Rev 2015; 115: 11718–11940.

[2] Mei J, Hong Y, Lam JWY, Qin A, Tang Y, Tang BZ. Aggregation-induced emission: the whole is more brilliant than the parts. Adv Mater 2014; 26: 5429–5479.

[3] Xu S, Duan Y, Liu B. Precise molecular design for high-performance luminogens with aggregation-induced emission. Adv Mater 2019; 32: 1903530.

[4] Zhang H, Zhao Z, Turley AT, Wang L, McGonigal PR, Tu Y, Li Y, Wang Z, Kwok RTK, Lam JWY, Tang BZ. Aggregate science: from structures to properties. Adv Mater 2020; 32: 2001457.

[5] Luo JD, Xie ZL, Lam JWY, Cheng L, Chen H, Qiu CF, Kwok HS, Zhan XW, Liu Y, Zhu D, Tang BZ. Aggregation-induced emission of 1-methyl-1,2,3,4,5-pentaphenylsilole. Chem Commun 2001; 18: 1740–1741.

[6] Tang BZ, Zhan X, Yu G, Lee PPS, Liu Y, Zhu D. Efficient blue emission from siloles. J Mater Chem 2001; 11: 2974–2978.

[7] Hong Y, Lam JWY, Tang BZ. Aggregation-induced emission. Chem Soc Rev 2011; 40: 5361−5388.

[8] Wang J, Mei J, Hu R, Sun JZ, Qin A, Tang BZ. Click synthesis, aggregation-induced emission, E/Z isomerization, self-organization, and multiple chromisms of pure stereoisomers of a tetraphenylethene-cored luminogens. J Am Chem Soc 2012; 134: 9956–9966.

[9] Chen Y, Lam JWY, Kwok RTK, Liu B, Tang BZ. Aggregation-induced emission: fundamental understanding and future developments. Mater Horiz 2019; 6: 428–433.

[10] Luo J, Song K, Gu FL, Miao Q. Switching of non-helical overcrowded tetrabenzoheptafulvalene derivatives. Chem Sci 2011; 2: 2029–2034.

[11] Lin Z, Qin A. Diverge from the norm. Nat Sci Rev 2014; 1: 22–24.

[12] Ding D, Li K, Liu B, Tang BZ. Bioprobes based on AIE fluorogens. Acc Chem Res 2013; 46: 2441–2453.

[13] Kwok RT, Leung CW, Lam JW, Tang BZ. Biosensing by luminogens with aggregation-induced emission characteristics. Chem Soc Rev 2015; 44: 4228–4238.

[14] Feng B, Liu B. Aggregation-Induced emission (AIE) dots: emerging theranostic nanolights. Acc Chem Res 2018; 51: 1404–1414.

[15] Vij V, Bhalla V, Kumar M. Hexaarylbenzene: evolution of properties and applications of multitalented scaffold. Chem Rev 2016; 116: 9565−9627.

[16] Islam M. M, Hu Z, Wang QS, Redshaw C, Feng X. Pyrene-based aggregation-induced emission luminogens and their applications. Mater Chem Front 2019; 3: 762−781.

[17] Figueira-Duarte TM, Müllen K. Pyrene-based materials for organic electronics. Chem Rev 2011; 111: 7260−7314.

[18] Feng X, Hu JY, Redshaw C, Yamato T. Functionalization of pyrene to prepare luminescent materials-typical examples of synthetic methodology. Chem -Eur J 2016; 22: 11898–11916.

[19] Oyamada T, Uchiuzou H. Lateral organic light-emitting diode with field-effect transistor characteristics. J Appl Phys 2005; 98: 74506.

[20] Wang CZ, Feng X, Kowser Z, Wu C, Akther T, Elsegood MRJ, Redshaw C, Yamato T. Pyrene-based color-tunable dipolar molecules: Synthesis, characterization and optical properties. Dyes Pigm 2018; 153: 125–131.

[21] Zhang Z, Xu B, Su J, Shen L, Xie Y, Tian H. Color-tunable solid-State emission of 2,2’-biindenyl‑based fluorophores. Angew Chem Int Ed 2011; 50: 11654−11657.

[22] Sonar P, Soh MS, Cheng YH, Henssler JT, Sellinger A. 1,3,6,8-tetrasubstituted pyrenes: solution-processable materials for application in organic electronics. Org Lett 2010; 12: 3292–3295.

[23] Son S, Dodabalapur A, Lovinger AJ, Galvin ME. Luminescence enhancement by the Introduction of disorder into poly(p-phenylene vinylene). Science 1995; 269: 376–378.

[24] Li YX, Yang XF, Miao JL, Sun GX. Substitution position and vinylene bond geometry modulating the fluorescence solvatochromism and aggregation-induced emission of (9-Anthryl)vinyl(1-pyrenyl)vinylbenzene isomers. J Phys Chem C 2016; 120: 21722–21729.

[25] Aragay G, Pons J, Merkoci A. Recent trends in macro-, micro-, and nanomaterial-based tools and strategies for heavy-metal detection. Chem Rev 2011; 111: 3433–3458.

[26] Chai Q, Wei J, Bai B, Wang H, Li M. Multiple iuminescent switching of pyrenyl-substituted acylhydrazone derivative. Dyes Pigm 2018; 152: 93–99.

[27] Xing C, Liu J, Chen F, Li Y, Lv C, Peng Q, Hou H, Li K. Diphenyl-1-pyrenylphosphine: photo-triggered AIE/ACQ transition with remarkable third-order nonlinear optical signal change. Chem Commun 2020; 56: 4220–4223.

[28] Zhao ZJ, Chen SM, Lam JWY, Lu P, Zhong YC, Wong KS, Kwok HS, Tang BZ. Creation of highly efficient solid emitter by decorating pyrene core with AIE-active tetraphenylethene peripheries. Chem Commun 2010; 46: 2221–2223.

[29] Zhao ZJ, Chen SM, Lam JWY, Wang ZM, Lu P, Mahtab F, Sung HHY, Williams ID, Ma Y, Kwok HS, Tang BZ. Pyrene-substituted ethenes: aggregation-enhanced excimer emission and highly efficient electroluminescence. J Mater Chem 2011; 21: 7210–7216.

[30] Zhang ZM, Zhao YZ, Zhang R, Zhang LF, Cheng WQ, Ni ZH. Design and synthesis of a new series of tetra(polycyclic aryl)ethenes: achieving aggregation-induced emission and efficient solid-state photoluminescence. Dyes Pigm 2015; 118: 95–101.

[31] Yang J, Guo QX, Wen XD, Gao XM, Peng Q, Li QQ, Ma DG, Li Z. Pyrene-based blue AIEgens: tunable intramolecular conjugation, good hole mobility and reversible mechanochromism. J Mater. Chem C 2016; 4: 8506–8513.

[32] Li YX, Yang XF, Miao JL, Sun GX. Substitution position and vinylene bond geometry modulating the fluorescence solvatochromism and aggregation-induced emission of (9-anthryl)vinyl(1-pyrenyl)vinylbenzene isomers. J Phys Chem C 2016; 120: 21722–21729.

[33] Katla J, Bhat HR, Jha PC, Ghalsasi PS, Kanvah S. α-Cyanostyrenes with pyrene scaffold: unique emission through aggregation. ChemistrySelect 2017; 2: 1902–1910.

[34] Karuppusamy A, Vandana T, Kannan P. Pyrene based chalcone materials as solid state luminogens with aggregation-induced enhanced emission properties. J Photochem Photobiol A 2017; 345: 11–20.

[35] Shellaiah M, Wu YH, Singh A, Raju MVR, Lin HC. Novel pyrene- and anthracene-based Schiff base derivatives as Cu^{2+} and Fe^{3+} fluorescence turn-on sensors and for aggregation induced emissions. J Mater Chem A 2013; 1: 1310–1318.

[36] Chai Q, Wei J, Bai BL, Wang HT, Li M. Multiple luminescent switching of pyrenyl-substituted acylhydrazone derivative. Dyes Pigm 2018; 152: 93–99.

[37] Shyamal M, Maity S, Mazumdar P, Sahoo G P, Maity R, Misra A. Synthesis of an efficient pyrene based AIE active functional material for selective sensing of 2,4,6-trinitrophenol. J Photochem Photobiol A 2017; 342: 1–14.

[38] Zhao ZJ, Li JH, Chen XP, Wang XM, Lu P, Yang Y. Solution-processable stiff dendrimers: synthesis, photophysics, film morphology, and electroluminescence. J Org Chem 2009; 74: 383–395.

[39] Huang J, Wu YR, Chen Y, Zhu Z, Yang XH, Yang CJ, Wang KM, Tan WH. Pyrene-excimer probes based on the hybridization chain reaction for the detection of nucleic acids in complex biological fluids. Angew Chem Int Ed 2011; 50: 401–404.

[40] Shi CX, Guo ZQ, Yan YL, Zhu SQ, Xie YS, Zhao YS, Zhu WH, Tian H. Self-assembly solid-state enhanced red emission of quinolinemalononitrile: optical waveguides and stimuli response. ACS Appl Mater Interfaces 2013; 5: 192–198.

[41] Feng X, Xu Z, Hu Z, Qi CX, Luo DX, Zhao XY, Mu ZF, Redshaw C, Lam JWY, Ma DG, Tang BZ. Pyrene-based blue emitters with aggregation-induced emission features for high-performance organic light-emitting diodes. J Mater Chem C 2019; 7: 2283–2290.

[42] Wang CZ, Noda Y, Wu C, Feng X, Venkatesan P, Cong H, Elsegood MRJ, Warwick TG, Teat SJ, Redshaw C, Yamato T, Multiple photoluminescence from pyrene-fused hexaarylbenzenes with aggregation-enhanced emission features. Asian J Org Chem 2018; 7: 444–450.

[43] Wang C, Li Z, Molecular conformation and packing: their critical roles in the emission performance of mechanochromic fluorescence materials. Mater Chem Front 2017; 1: 2174–2194.

[44] Lin YL, Chen G, Zhao LF, Yuan WZ, Zhang YM, Tang BZ, Diethylamino functionalized tetraphenylethenes: structural and electronic modulation of photophysical

properties, implication for the CIE mechanism and application to cell imaging. J. Mater Chem C 2015; 3: 112–120.

[45] G

[46] Gopikrishna P, Meher N, Iyer PK, Functional 1,8-naphthalimide AIE/AIEEgens: recent advances and prospects. ACS Appl Mater Interfaces 2018; 10: 12081−12111.

[47] Shao SY, Wang LX, Through-space charge transfer polymers for solution‐processed organic light‐emitting diodes. Aggregate 2020; 1: 45–56.

[48] Gulyani A, Dey N, Bhattacharya S, A unique self-assembly-driven probe for sensing a lipid bilayer: ratiometric probing of vesicle to micelle transition. Chem Commun 2018; 54: 5122–5125.

[49] Zhang YY, He BR, Liu JK, Hu SM, Pan LX, Zhao ZJ, Tang BZ, Aggregation-induced emission and the working mechanism of 1-benzoyl and 1-benzyl pyrene derivatives. Phys Chem Chem Phys 2018; 20: 9922–9929.

[50] Wang Q, Zhang Q, Zhang QW, Li X,, Zhao CX, Xu TY, Qu DH, Tian H, Color-tunable single-fluorophore supramolecular system with assembly-encoded emission. Nat Commun 2020; 11: 158.

[51] Luo XL, Li JN, Li CH, Heng LP, Dong YQ, Liu ZP, Bo ZS, Tang BZ, Reversible Switching of the emission of diphenyldibenzofulvenes by thermal and mechanical stimuli. Adv Mater 2011; 23: 3261−3265.

[52] Safin DA, Babashkina MG, Mitoraj MP, Kubisiak P, Robeyns K, Bolte M, Garcia Y, An intermolecular pyrene excimer in the pyrene-labeled N-thiophosphorylated thiourea and its nickel(ii) complex. Inorg Chem Front 2016; 3: 1419–1431.

[53] Feng X, Qi CX, Feng HT, Zhao Z, Sung HHY, Williams ID, Kwok RTK, Lam JWY, Qin A, Tang BZ, Dual fluorescence of tetraphenylethylene-substituted pyrenes with aggregation-induced emission characteristics for white-light emission. Chem Sci 2018; 9: 5679–5687.

[54] Wang CZ, Pang ZJ, Yu ZD, Zeng ZX, Zhao WX, Zhou ZY, Redshaw C, Yamato T, Short axially asymmetrically 1,3-disubstituted pyrene-based color-tunable emitters: synthesis, characterization and optical properties. Tetrahedron 2021; 78: 131828.

[55] APEX 2 & SAINT (2012), software for CCD diffractometers. Bruker AXS Inc Madison, USA.

[56] Sheldrick GM, Acta Crystallogr 2008; A64: 112.

[57] Sheldrick GM, Acta Cryst 2015; A71: 3.

[58] Sheldrick GM, Acta Cryst 2015; C71: 3.